Low-lying states in ^{219}Ra and ^{215}Rn: Sampling microsecond α-decaying nuclei

A. Såmark-Roth *et al.*

Low-lying states in ^{219}Ra and ^{215}Rn: sampling microsecond α-decaying nuclei

A. Såmark-Roth,[1] L.G. Sarmiento,[1] D. Rudolph,[1] J. Ljungberg,[1] B.G. Carlsson,[1] C. Fahlander,[1]
U. Forsberg,[1] P. Golubev,[1] I. Ragnarsson,[1] D. Ackermann,[2,*] L.-L. Andersson,[3] M. Block,[2,3,4] H. Brand,[2]
D.M. Cox,[5,1] A. Di Nitto,[4] Ch.E. Düllmann,[2,3,4] K. Eberhardt,[3,4] J. Even,[3,†] J.M. Gates,[6] J. Gerl,[2]
K.E. Gregorich,[6] C.J. Gross,[7] R.-D. Herzberg,[5] F.P. Heßberger,[2,3] E. Jäger,[2] J. Khuyagbaatar,[2,3]
B. Kindler,[2] I. Kojouharov,[2] J.V. Kratz,[4] J. Krier,[2] N. Kurz,[2] B. Lommel,[2] A. Mistry,[5,3] C. Mokry,[3,4]
J.P. Omtvedt,[8] P. Papadakis,[5] J. Runke,[2,4] K. Rykaczewski,[7] M. Schädel,[2] H. Schaffner,[2] B. Schausten,[2]
P. Thörle-Pospiech,[3,4] N. Trautmann,[4] T. Torres,[2] A. Türler,[9] A. Ward,[5] N. Wiehl,[3,4] A. Yakushev [2].

[1] *Lund University, 22100 Lund, Sweden*
[2] *GSI Helmholtzzentrum für Schwerionenforschung GmbH, 64291 Darmstadt, Germany*
[3] *Helmholtz Institute Mainz, 55099 Mainz, Germany*
[4] *Johannes Gutenberg-Universität Mainz, 55099 Mainz, Germany*
[5] *University of Liverpool, Liverpool L69 7ZE, United Kingdom*
[6] *Lawrence Berkeley National Laboratory, Berkeley, California 94720, USA*
[7] *Oak Ridge National Laboratory, Oak Ridge, Tennessee 37831, USA*
[8] *University of Oslo, 0315 Oslo, Norway and*
[9] *Paul Scherrer Institute and University of Bern, 5232 Villigen, Switzerland*
(Dated: August 13, 2018)

Short-lived α-decaying nuclei 'North-East' of ^{208}Pb in the chart of nuclides were studied using the reaction ^{48}Ca + ^{243}Am with the decay station TASISpec at TASCA, GSI Darmstadt. Decay energies and times from pile-up events were extracted with a tailor-made pulse shape analysis routine and specific α-decay chains were identified in a correlation analysis. Decay chains starting with the even-even ^{220}Ra and its odd-A neighbors, ^{219}Fr, and ^{221,219}Ra, with a focus on the ^{219}Ra→^{215}Rn decay, were studied by means of α-γ spectroscopy. A revised α-decay scheme of ^{219}Ra is proposed, including a new decay branch from a previously not considered isomeric state at 17 keV excitation energy. Conclusions on nuclear structure are drawn from the experimental data, aided by Geant4 simulations and a discussion on theoretical calculations.

I. INTRODUCTION

In the chart of nuclides the majority of α-decaying nuclei are found 'North-East' of the heaviest stable isotope in existence, namely ^{208}Pb. Here Gamow's theory of α decay explains the very long half-lives of ^{232}Th and ^{238}U and simultaneously the existence of very short-lived α-decaying nuclei, just above the magic neutron number $N = 126$. In fact the most short-lived α-decaying isotopes known to date are those that decay as $N = 128 \rightarrow 126$. Their short half-lives can be explained with the increased stability at the $N = 126$ shell closure leading to large disintegration energies (Q_α). One decay chain that crosses $N = 128$ is $^{219}_{88}$Ra$_{131}$ →$^{215}_{86}$Rn$_{129}$ →$^{211}_{84}$Po$_{127}$.

Over the years, several measurements of the decay ^{219}Ra→^{215}Rn have been made. The decay scheme resulting from previous measurements is presented in Fig. 1. Following the decay of ^{227}U, two main α-decay branches of both the ^{223}Th→^{219}Ra and ^{219}Ra→^{215}Rn decays were observed in the 1960s [1, 2]. The half-life of ^{219}Ra and ^{215}Rn from these measurements, 10(3) ms and 2.30(10) μs, respectively, remain accepted at ENSDF [3–5]. In the late 1980s, further decay spectroscopy experiments were performed to study these nuclei by ob-

serving the decay of ^{223}Th and its daughters produced in the ^{208}Pb(^{18}O, 3n) reaction [6, 7]. These experiments led to the establishment of several low-lying states in both ^{219}Ra and ^{215}Rn. Further, a strong $M1$ transition with an energy of 316 keV was observed connecting an excited state and the ground state of ^{215}Rn. Before the 1980s, due to a measured unhindered α-decay to ^{211}Po, the ground-state spin of ^{215}Rn was assigned as $I^\pi = 9/2^+$. By means of angular correlation measurements, Ref. [8] limited the possible spin values of the above-mentioned ^{215}Rn excited state to $I^\pi = 7/2^+$ or $11/2^+$. Motivated by a small hindrance factor for the decay into the excited state, the ^{219}Ra ground-state spin was further assigned to be the same, i.e. $7/2^+$ or $11/2^+$ [8].

In attempts to determine the ground-state spin of ^{219}Ra, further in-beam high-spin experiments were conducted [9, 10]. Among the different measurements, only a few excited states and transitions were common. To date, ^{219}Ra is predicted to lie at or near the limit of where stable octupole deformation exists [11]. The varying experimental level schemes might have been due to the complications octupole deformation brings to the nuclear structure. Nevertheless, by means of conversion electron-γ ray coincidences, Riley *et al.* [12] managed to connect the contradictory level schemes. Supported by theoretical calculations, the ground-state spin of ^{219}Ra was inferred to be $I^\pi = 7/2^+$.

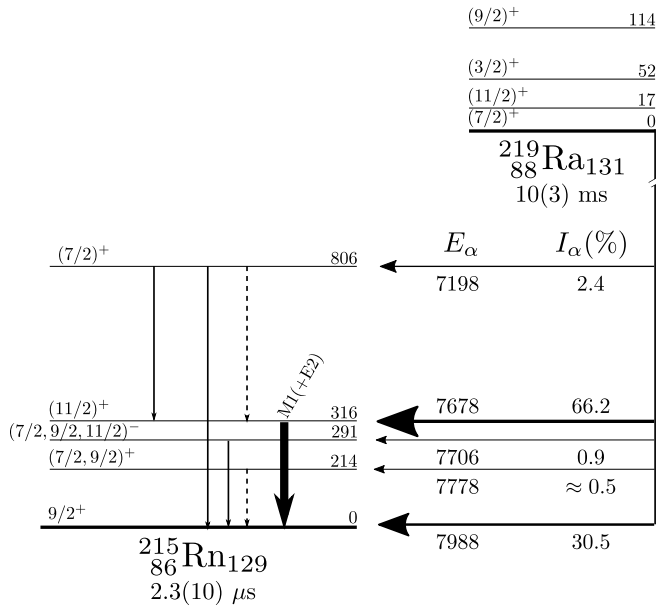In the most up-to-date version of the decay scheme, the first two low-lying excited states in ^{219}Ra are the 17 keV

FIG. 1: Decay scheme of ^{219}Ra$\rightarrow$^{215}Rn adopted from Ref. [3–5]. Level energy labels are in keV and α-energies in MeV. The widths of the arrows indicate the intensity of the transition and dashed lines show tentative transitions. The ^{219}Ra levels are based on Refs. [10, 12, 13]. The α-decay scheme is based on Refs. [1, 6, 7].

of these nuclei. Firstly, with standard analog electronics, pile-up events are created by two subsequent α decays occuring within a few microseconds. Pile-up data aggravate spectroscopic studies. However, the advent and use of sampling electronics, i.e. digitizing the preamplified pulse with a sampling frequency of some 50-100 MHz, allows selecting and studying such events. Our approach on how to deal with such events is presented in Sec. III. Secondly, several different radioactive species arrive at the detector set-up and naturally, they assume very similar decay characteristics. In this paper, an analysis of α_1-α_2-α_3 correlations, described in Sec. IV, is utilised as a method to efficiently filter out one decay path at a time. The employment of both methods can lead to improved, if not revised, experimental decay schemes of these microsecond α-decaying isotopes. Note that many of these isotopes have not been studied since the 1970s.

The experimental results of the current paper are presented in Sec. V. Measured decay energies and half-lives of chains starting from the even-even ^{220}Ra and its odd-A neighboring isotopes ^{219}Fr, ^{221}Ra and ^{219}Ra are compared with previous measurements. Following this, the ^{219}Ra$\rightarrow$^{215}Rn decay is investigated in great detail with coincident photon data and by means of Geant4 simulations [18]. In Sec. VI, this decay path is confronted with contemporary α-decay models. The findings are summarized in Sec. VII.

II. EXPERIMENT

At the GSI Helmholtzzentrum für Schwerionenforschung, the Universal Linear Accelerator (UNILAC) provided an intense beam of ^{48}Ca ions, at 5.4-5.5 MeV per nucleon and with a pulse structure of 5 ms beam on, 15 ms beam off. The ^{48}Ca ions impinged on thin ^{243}Am$_2$O$_3$ target segments in front of the gas-filled separator TASCA [19–21], which was optimised to transmit and focus moscovium (element $Z = 115$) fusion-evaporation residues into the detector set-up TASISpec [22]. In brief, TASISpec is a cubic arrangement of five double sided silicon strip detectors (DSSSDs), closely surrounded by five large, composite germanium detectors for high-resolution and high efficiency α-photon coincidence spectroscopy. For more detailed information concerning all parameters of the experiment as well as the detector set-up and detector calibrations, we refer to Refs. [15–17] and references therein.

Short-lived non-fusion reaction products comprise a significant part of the 100/s beam-on trigger rate. For the study of these isotopes by means of high resolution α-decay spectroscopy, digitizing the preamplifier pulses is essential. In the experiment, the preamplified signals were recorded (see Supplemental Material) by 12 bit, 60 MHz fast sampling ADCs [23, 24] for the strips on the p-sides of the silicon detectors. In contrast to analog electronics systems, pulse-shape analysis, here based on offline software implementations, enable the extraction

and 52 keV levels with tentative spin assignments $11/2^+$ and $3/2^+$, respectively, see Fig. 1. At the time when the previous α-decay spectroscopy experiments of ^{219}Ra were conducted, this low-lying structure was not known. An excited state at 17 keV implies a small electromagnetic decay probability. Furthermore, differences in nuclear shape and structure between the ground state and the 17-keV state (cf. Ref. [12] and Sec. VI) may lead to significant additional hindrance for electromagnetic decays [14]. Thus, it is possible to consider the 17-keV state as an isomeric α-decaying state in ^{219}Ra. In this article, the existence of such an isomeric α-decaying state is confronted with α-γ spectroscopy and contemporary nuclear structure and α-decay models. The results shed light on the ground-state spin of ^{219}Ra.

Data for the present study stem from an experiment which aimed at α-photon coincidence spectroscopy of α-decay chains associated with element 115, moscovium (Mc) [15]. A brief revision of the relevant experimental details is given in Sec. II. Besides giving rise to the observation of 30 decay chains from ^{287,288,289}Mc [16, 17], this large high-quality α-photon data set also comprises a significant amount of information on non-fusion reaction background channels.

Relevant for the current work are the non-fusion products in the ^{48}Ca+^{243}Am reaction with proton numbers $Z \sim 88 - 90$ which α decay in correlated chains towards the $N = 126$ shell closure. These decay chains typically comprise at least one α-decay step with a half-life less than a few microseconds. Two issues arise for the study

of energies and times from pile-up events.

III. DATA ANALYSIS – HANDLING OF PILE-UP EVENTS

With dedicated algorithms applied to preamplifier trace data, it is possible to resolve the pile-up or multi-pulse traces. This procedure gives access to decay energies and lifetimes of short-lived α-decaying nuclei. For instance, in Refs. [23, 25–27], this technique was utilized for the study of very unstable, neutron-deficient α-emitting nuclei.

Established procedures to extract energies from digitized waveforms include software trapezoidal filters and moving window deconvolution (MWD) algorithms [28–32]. A typical MWD-implementation consists of three steps: *(i)* the exponentially decaying behaviour of the preamplifier signal is corrected for. The effect of this deconvolution is that the signal transforms into a step-like function. The operation allows for a more accurate measure of the value of the signal amplitude. *(ii)* The baseline will rise for subsequent pulses in a pile-up trace. To restore the baseline values, the step-pulse is shortened with an m-step differentiation of the deconvolved signal. This procedure is called differentiation and results in box-like pulses of the pile-up signal. *(iii)* To obtain a more precise value for the signal amplitude a moving average (with a width w) is applied. The moving average of a box-like pulse renders a trapezoidal pulse for $w < m$. A pulse amplitude is extracted as the averaged height of the trapezoid above the baseline.

In case of single-pulse traces it is rather straightforward to find the optimal implementation of the MWD parameters for a given detector. For intense, single α-decay transitions, FWHM of $19\,\mathrm{keV}$ and $25\,\mathrm{keV}$ are achieved for $E_\alpha \sim 6\,\mathrm{MeV}$ and $E_\alpha \sim 8\,\mathrm{MeV}$, respectively, for the full experimental data set. However, in the case of pile-up traces the time difference between the intrinsic pulses can vary substantially. The consequence is that every single pile-up trace needs a dedicated treatment. For example, the time for the start and end of each pulse within a pile-up trace needs to be determined before an optimal choice of MWD parameters, such as m and w, can be made. Nevertheless, due to the vast amount of data, an automated software algorithm is inevitable even for this special type of analysis. The implemented algorithm in this work is novel in the sense that it first identifies and labels pile-up traces in the data stream. For any such pile-up trace it then determines MWD parameters tailored for optimal time and energy resolution for each pulse. The method yields distinct peaks as exemplified by the energy spectrum in Fig. 3(a). Note that the FWHM of the peak at $7.98\,\mathrm{MeV}$ in Fig. 3(c) remains at $23\,\mathrm{keV}$. For examples of pile-up traces and details of the method we refer to the Supplemental Material and Ref. [33].

TABLE I: General and specific search criteria for correlations between implanted reaction products (*imp*) and subsequent α decays, α_1-α_2-α_3. The criteria include α-particle energies and correlation times for each step. Restrictions concerning beam status are indicated. See text for further details.

	General	Specific^a	Beam
E_{imp}	[0.5, 30] or [70, 120] MeV		ON
E_{α_1}	[6.0, 11.0] MeV	[7.0, 9.0] MeV	OFF
E_{α_2}	[6.0, 11.0] MeV	[8.0, 9.0] MeV	OFF
E_{α_3}	–	[7.3, 7.5] MeV	ON/OFF
$\Delta t_{imp\text{-}\alpha_1}$	[0.1, 100] ms	[0.1, 100] ms	
$\Delta t_{\alpha_1\text{-}\alpha_2}$	[0.0, 50.0] µs	[0.0, 13.0] µs	
$\Delta t_{\alpha_2\text{-}\alpha_3}$	–	[0.005, 3.5] s	

^{a} Correlation criteria matched to the $^{219}\mathrm{Ra} \rightarrow {}^{215}\mathrm{Rn} \rightarrow {}^{211}\mathrm{Po}$ decay chain.

IV. CORRELATION ANALYSIS

The signals of implanted ions (*imp*) and subsequent emissions of α-particles terminating with fission in the same detector pixel serves as a tagging technique in the identification of superheavy nuclei created in fusion-evaporation reactions. If fission is disregarded, conceptually the same technique can be employed to study other short-lived α-decaying nuclei. This method, referred to as correlation analysis, was applied for the current experiment on the moscovium decay chains [15–17] and is likewise applied in the present work.

General and specific search criteria for imp-α_1-α_2-α_3 correlations are presented in Table I. The imp-α_1-α_2 correlation search produces the correlation spectrum presented in Fig. 2(a). In Fig. 2(b,c) measured decay energies for $^{219}\mathrm{Ra}$ and $^{215}\mathrm{Rn}$ are indicated. Contaminating data surround and overlap the peaks of interest. This is expected since no specific isotope separation has been made. In the case of the $^{219}\mathrm{Ra}$ and $^{215}\mathrm{Rn}$ study, this is a complication which is eminent: The odd-odd $^{218}\mathrm{Fr} \rightarrow {}^{214}\mathrm{At}$ chain has similar lifetimes and overlapping decay energies. To overcome this problem, α_1-α_2-α_3 correlations are used, as the third members in the two chains, $^{211}\mathrm{Po}$ and $^{210}\mathrm{Bi}$, have very different decay properties. This way, data of specific decay chains can be separated and clean and unambiguous spectra, exemplified in Fig. 3, can be obtained. It should be noted that, very few $^{223}\mathrm{Th}$ nuclei were identified in the data set and complementary $^{223}\mathrm{Th} \rightarrow {}^{219}\mathrm{Ra} \rightarrow {}^{215}\mathrm{Rn}$ correlated chains could not be utilized in the study of the $^{219}\mathrm{Ra} \rightarrow {}^{215}\mathrm{Rn}$ decay.

Correlation times (denoted $\Delta t_{imp\text{-}\alpha_1}$ and $\Delta t_{\alpha_i\text{-}\alpha_{i+1}}$) are set to cover the 98% confidence band of the expected lifetime distribution derived from tabulated half-life values [3]. Search conditions for E_{α_i} are initially guided by tabulated values. Final energy gates are set to the full width at 1/3 of maximum of peaks in the measured
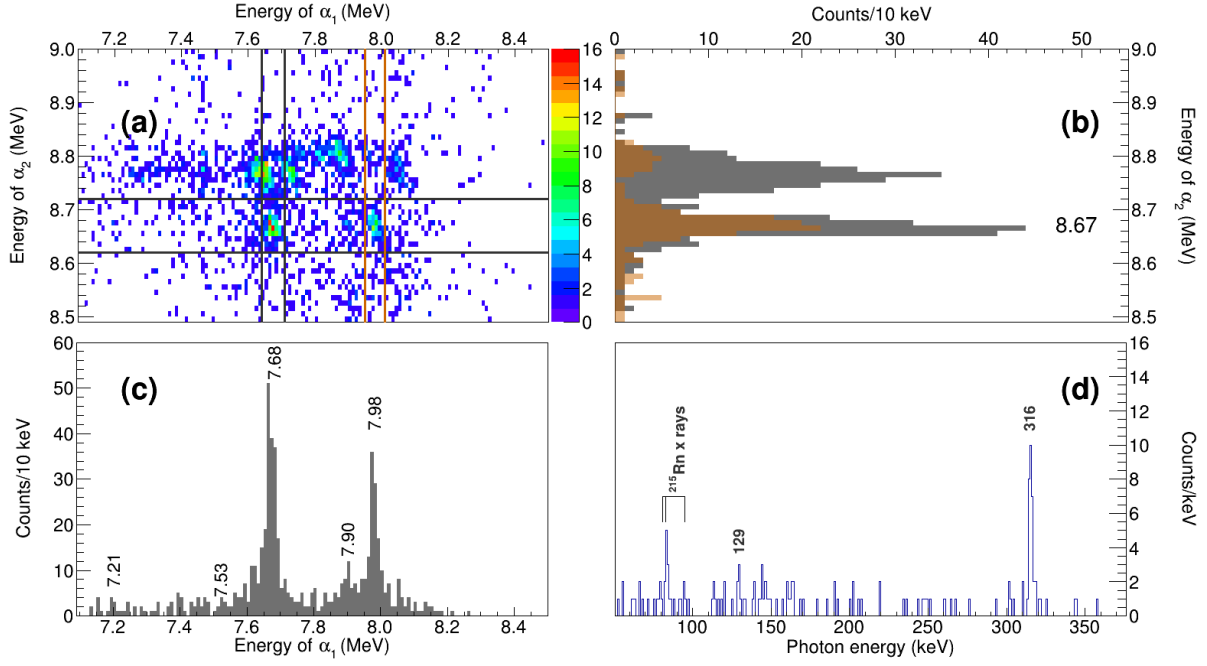
FIG. 2: **(a)** α_1-α_2 correlation spectrum for the general imp-α_1-α_2 criteria presented in Table I. Energy gates for the ^{219}Ra$\rightarrow^{215}$Rn correlation chain are drawn with horizontal and vertical lines. Panels **(b)** and **(c)** illustrate projections based on the energy gates of α_1 and α_2 (with corresponding colors), respectively. Possible α-energy peaks for ^{219}Ra and ^{215}Rn in MeV are indicated. Panel **(d)** presents photons in prompt coincidence with α_1, selected according to the horizontal lines in panel (a). Identified photon peaks are labelled.
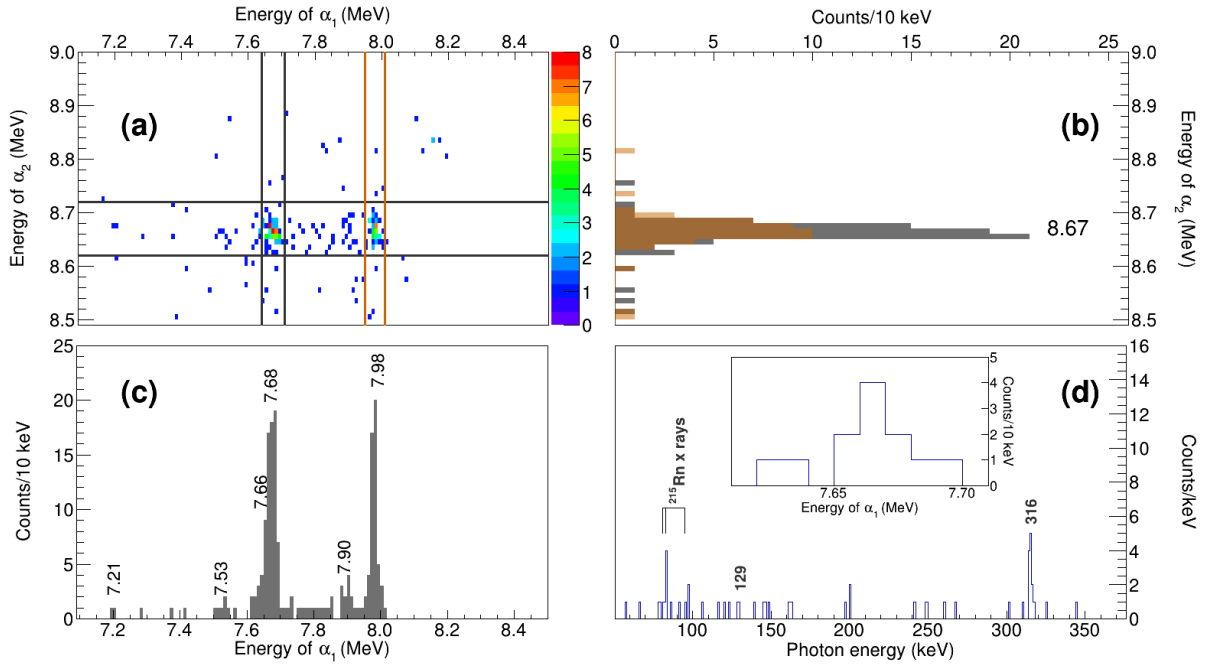

FIG. 3: Same as Fig. 2 but based on the specific α_1-α_2-α_3 criteria matching the ^{219}Ra$\rightarrow^{215}$Rn$\rightarrow^{211}$Po decay chain (see Table I). The inset in panel **(d)** presents α particles in coincidence with 316 keV photons.

energy spectra.

In the course of the analysis the competition between maximizing statistics but minimising contaminating data acted as guidance. Including preceding or subsequent α-decays to α_1-α_2 correlations of the decay path of interest showed the best results.

V.   RESULTS

Figure 1 shows the decay scheme of ^{219}Ra$\rightarrow^{215}$Rn established on the basis of previous measurements. Besides the peculiar ground-state spin $7/2^+$ of ^{219}Ra [12], the most interesting feature for the present work is the existence of an excited state in ^{219}Ra at only 17 keV in excitation energy. The Weisskopf estimate for an electromagnetic decay between states differing by an energy of 17 keV predicts a half-life of 6 ms for an $E2$ transition, which reduces to 0.2 µs due to a conversion coefficient of $\alpha_{tot} \approx 30000$ [34]. However, differences in shape, single-particle composition, and angular momentum couplings between ground state and 17 keV state (cf. Ref. [12] and Sec. VI) can introduce significant additional hindrance for the electromagnetic decay of the 17 keV state [14], such that the existence of two α-decaying states in ^{219}Ra is worth to be considered. Since previous decay spectroscopy studies were conducted prior to the establishment of the 17 keV level, the above-mentioned scenario was not considered. Thus the excited state at 17 keV may then call for a re-evaluation of the α-decay scheme. The decay scheme proposed by this work is presented in Fig. 4(a).

A.   Experimental − ^{219}Ra$\rightarrow^{215}$Rn decay

Figures 3(c) and 3(d) present the total α-correlation spectrum of ^{219}Ra and photons coincident with its decay. Our work agrees with the placement of the 316 keV transition which connects the 7.68 MeV and 7.98 MeV α-decay branches. The electron from a K-conversion for the 316 keV deexcitation carries an energy of $\sim$ 220 keV [34]. A sum peak of the conversion electron and the 7.68 MeV α-decay is the source of the 7.90 MeV peak which is visible in the particle spectrum (see Fig. 3(c)).

Further, two small peaks at 7.53 MeV and 7.21 MeV are present in the α-particle correlation spectrum in Fig. 3(c). In the α-photon coincidence spectrum in Fig. 3(d), the two photon counts at 129 keV stem from prompt coincidences with the seven counts in the 7.53 MeV α group in Fig. 3(c). A 7.53 MeV α-branch has not been proposed in earlier experiments, but the energy difference of 0.13 MeV between a 7.66 MeV (introduced in the following paragraph) and 7.53 MeV peak supports its existence. There are two counts at 7.21 MeV in Fig. 3, which support the previously measured α-decay branch into a state at 806 keV in ^{215}Rn [3].

As can be seen in Fig. 3(c), the peak at 7.68 MeV is significantly wider than the 7.98 MeV peak. It is reasonable to argue that the 7.68 MeV peak in fact comprises not one but two α-decay branches. The additional branch has an energy of 7.66 MeV (see Fig. 3(c)). Both α-decay branches are in coincidence with the 316 keV γ ray (see inset in Fig. 3(d)). As these are prompt coincidences (cf. Fig. 2 in Ref. [16]), this indicates that there are two different α-decaying states in the mother nucleus ^{219}Ra which enter the same excited state in the daughter ^{215}Rn.

B.   Geant4 simulations − ^{219}Ra$\rightarrow^{215}$Rn decay

The proposed two α-decaying states in ^{219}Ra were studied more closely by means of Geant4 simulations [18]. By comparing the simulated and experimental data, confidence in the nuclear structure results can be obtained. The full experimental set-up used in the experiment, TASISpec, has been implemented in a virtual Geant4 environment [35–37]. To resemble the experimental conditions, in the present simulation, a beam of ^{219}Ra was directed towards the center of the implantation DSSSD, perpendicular to the detector plane and spatially distributed as a 2D Gaussian with $\sigma_{x,y} = 1$ cm. The beam energy was set to 80(5) MeV, corresponding to observed implantation energies of the non-fusion reaction products. The simulation was restricted to the decay of ^{219}Ra. Finally, the particle and photon coincidence spectra were normalised with a common factor derived from the experimental particle spectrum.

In the simulations, the complexity of the decay scheme was built up systematically as further decay branches and nuclear transitions were added. In the process, the angular momentum and multipolarity of the transitions were optimized through comparisons of x-ray, γ-ray, and α-particle yields. Initially, two simulation scenarios were considered: i) The 7.68 MeV α-branch and a 316 keV γ ray of pure $M1$ and ii) the 7.53 MeV α-branch and a 129 keV $E2$ transition. Neither of the two scenarios were able to reproduce the width of the experimental 7.68 MeV peak.

In further simulations, two α-branches of around 7.67 MeV separated by 20 keV were included as well as the 7.98 MeV branch. The absolute energy and the relative intensity of the two α-branches of around 7.67 MeV were varied to obtain the best agreement between the experiment and the simulation. Figure 5 presents the resulting particle and photon spectra of the best simulation of the revised level scheme developed in the present work. In the figure, this simulation is compared to a Geant4 simulation with the hitherto evaluated decay scheme as shown in Fig. 1) and the experimental data. It can be observed that the simulated particle spectrum (see Fig. 5(a) as a dashed red line) based on the evaluated nuclear data does not reproduce the shape of the 7.68 MeV peak well. Although a decay branch with an energy of 7.71 MeV exists in the simulation of the evaluated decay level scheme,
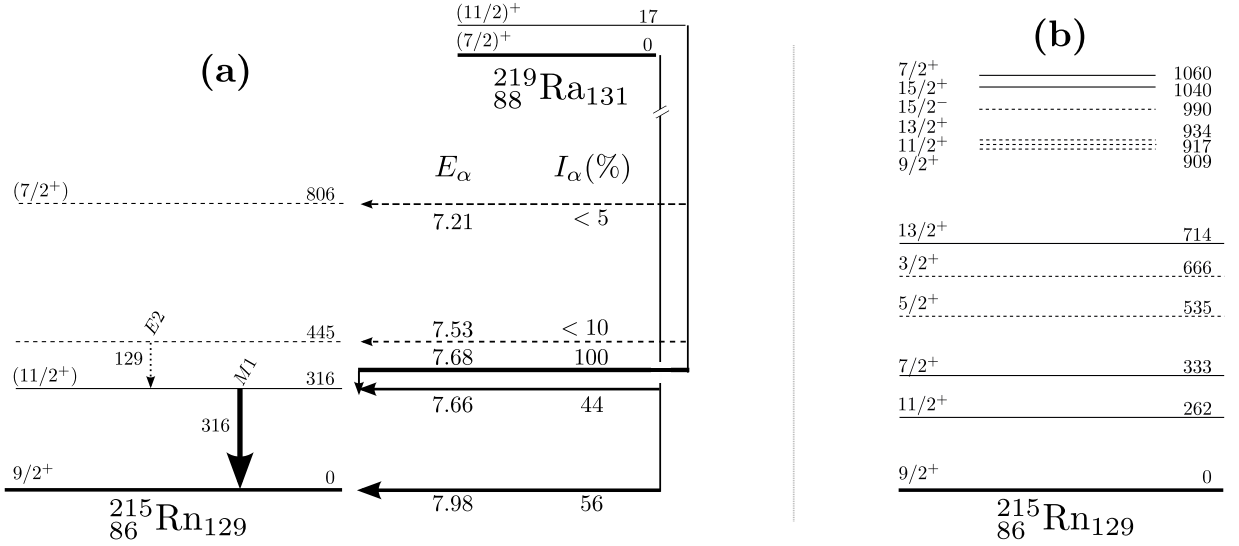
FIG. 4: **(a)** Decay scheme proposed by the current work. Levels in ^{219}Ra and ^{215}Rn are given in keV while the α-energies E_α are presented in MeV. Dashed and dotted lines indicate tentative assignments. **(b)** Levels in ^{215}Rn predicted by shell-model calculations. Experimentally observed states are indicated by straight lines.
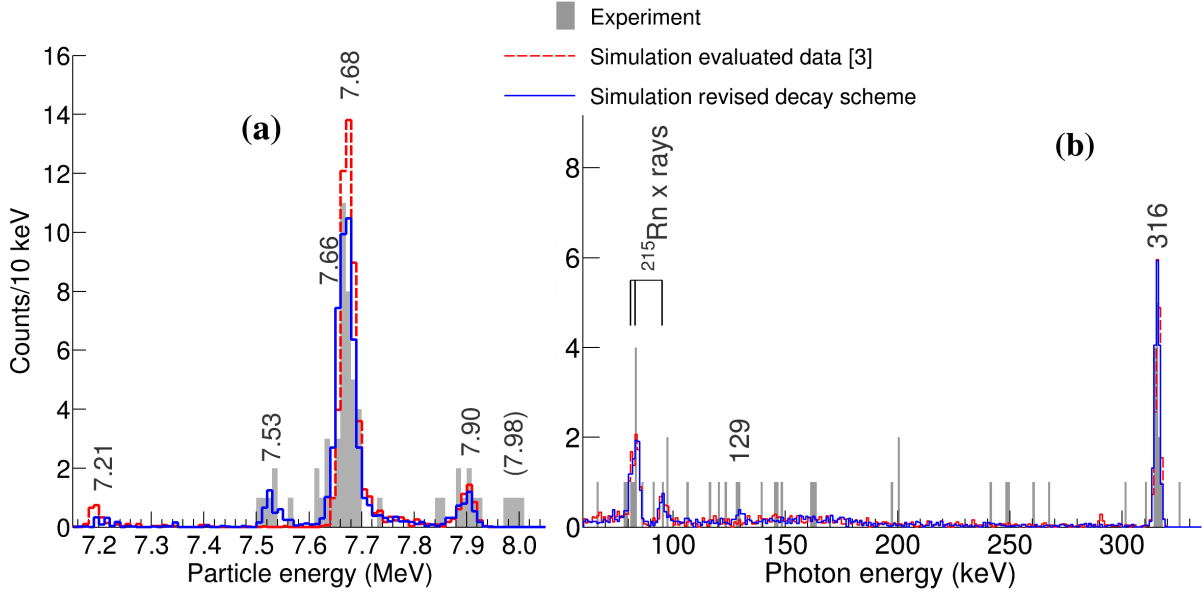

FIG. 5: Experimental and Geant4 simulated particle **(a)** and photon **(b)** coincidence spectra with a 10 keV and 1 keV binning, respectively. Two different simulated spectra are given. The first is based on evaluated nuclear structure data (see Fig.1) of the ^{219}Ra$\rightarrow^{215}$Rn decay (red dashed line). The second is based on the revised decay scheme proposed in this work (blue line). For further discussions see text.

it is far too small to affect the width of the peak. The simulated photon spectra in Fig. 5(b) are consistent for the x-ray yield, and the intensity of the 316 keV peak.

C. Summary of experiment and simulation – ^{219}Ra$\rightarrow^{215}$Rn decay

Detailed nuclear structure properties and results derived from this work are presented in Table II. The decay

energies E_α and the branching ratios have been guided by comparisons between the simulation and the experiment. Due to its larger α energy, we suggest that the 7.68 MeV branch stems from a decay of the 17 keV isomeric state, and that the 7.66 MeV branch is a decay channel of the ground state of ^{219}Ra. In addition, the 7.98 MeV branch is proposed to originate from the ^{219}Ra ground state as well. However, this cannot be motivated by the experimental observations alone. Despite the fact that the total Q_α value for the 7.66 MeV branch matches the Q_α of the
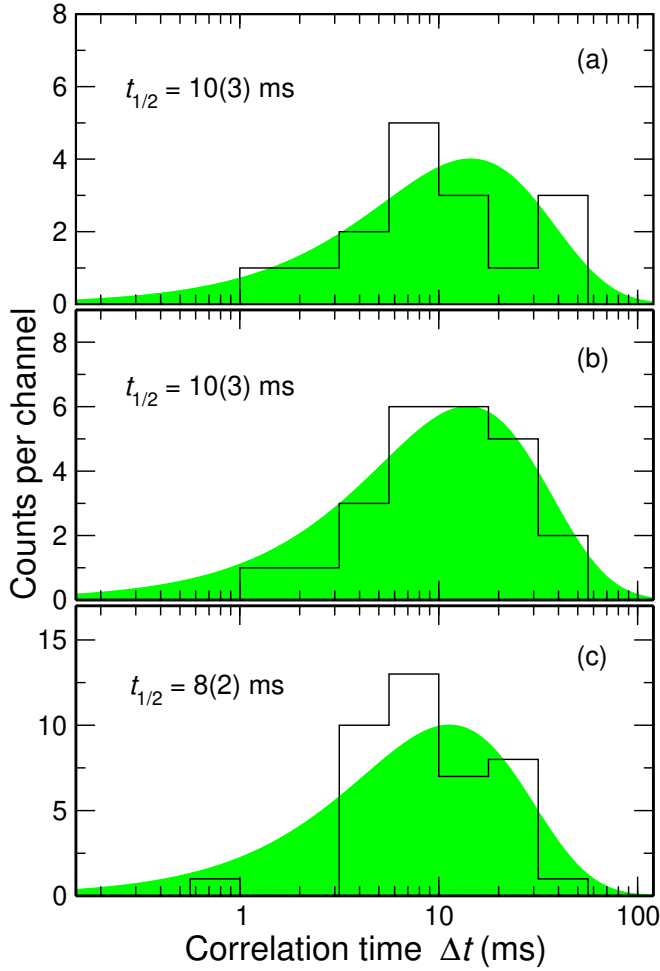
FIG. 6: Logarithmic distributions of correlation times for the 7.66 MeV (panel a), 7.68 MeV (panel b) and 7.98 MeV (panel c) branches of the ^{219}Ra→^{215}Rn α-decay.

TABLE II: Detailed properties of the ^{219}Ra → ^{215}Rn α decay in (a) and γ decay in (b) obtained in this work. **(a)** E_i and E_f represents initial and final states of the α-decay in ^{219}Ra and ^{215}Rn, respectively. Q_α includes the energy of possible electromagnetic transition reaching the ground state in ^{215}Rn. The half-lives, $t_{1/2}$, have been calculated according to the unbinned maximum likelihood method laid out in Ref. [38] in the frequentist inference. If feasible, the branching ratios have been derived from the simulation. **(b)** The experimental internal conversion coefficient for the K-shell, α_K, was calculated from the intensity relation between measured x and γ rays. The mixing ratio was calculated on the basis of the obtained α_K and computed internal conversion coefficients with BrIcc [34]. The multipole order σL of the transition was guided by simulations.

(a) α decay of ^{219}Ra

		^{219}Ra			^{215}Rn
E_i (keV)	$t_{1/2}$ (ms)[b]	E_α (MeV)	I_α[a] (%)	Q_α (MeV)	E_f (keV)
17	10(3)	7.68(2)[a]	100	8.14(2)[a]	316
0	10(3)	7.66(2)[a]	44(11)	8.13(2)[a]	316
0	8(2)	7.98(1)	56(11)	8.13(1)	0
		7.53(2)	< 10	8.10(2)	445
		7.21(2)	< 5	8.15(2)	806

(b) γ decay in ^{215}Rn

E_γ (keV)	Level (keV)	α_K	δ^2 (E2/M1)	σL[a]
316(1)	316	~ 0.5	~ 0	M1
129(1)	445			E2

[a]Guided by the simulation.
[b]Logarithmic distributions of correlation times are presented in Fig. 6.

7.98 MeV slightly better, it is not significant, see Table II. Furthermore, the calculated half-lives for the 7.66 MeV, 7.68 MeV, and 7.98 MeV branches cannot be separated with confidence, as can also be seen from Fig. 6 where the correlation time distributions for the three branches are presented. Rather, this aspect of the proposed decay scheme of ^{219}Ra is justified by theoretical calculations for the α decay, which are presented in the following section. The branching ratios of the 7.21 MeV and 7.53 MeV α-decay branches have only been given overall upper limits. This is because the data in the current work are not sufficient to define their origin, i.e. whether they stem from the ground state, the isomeric state, or both states. That being said, as the current analysis relies on direct production of ^{219}Ra, it is possible that the 7.53 MeV α-particles are emitted by the isomeric state, only. This offers an explanation to the fact that this decay branch was not observed in the decay study of ^{223}Th in Ref. [7].

Properties of the measured γ decays in ^{215}Rn are given in Table II(b). The best reproduction of the intensity of the 7.90 MeV sum-peak in the simulation was obtained

when the 316 keV transition was set to $M1$. Refs. [6, 7] have also concluded that the 316 keV transition is a pure $M1$. A rough calculation of the mixing ratio based on measured and calculated [34] conversion coefficients further supports this result. In the simulation, a 129 keV $E2$ transition best reproduced the experimental data as an $M1$ transition had too large of a conversion coefficient.

To summarize, previous decay spectroscopy studies of the ^{219}Ra→^{215}Rn decay have relied on α-γ coincidences to deduce their level schemes [6, 7] With the limited statistics in the present work it is not possible to either rule out or support the weak 7.706 MeV and 7.778 MeV branches which have been suggested in previous studies (see Fig. 1). In contrast to the previous experiments an efficient isotope separation, rendering clean data, has been made in this work producing the revised scheme presented in Fig. 4(a).

TABLE III: Compiled data of α-decay chains starting with the even-even ^{220}Ra or its odd-A neighbouring isotopes ^{219}Fr, ^{221}Ra and ^{219}Ra. The second column presents the correlation search used. Results obtained in this work are presented in the third column and corresponding tabulated values are given in the fourth column. Only ground-state to ground-state decays are considered.

Nucleus	Correlation	Present Work	Ref. [3]
		E_α (MeV) $t_{1/2}$	
^{219}Ra	(imp^b)-α_1^a-α_2-(α_3)	see Table II	
^{215}Rn	α_1-α_2^a-(α_3)	8.67(1) 2.5(3) µs	8.674(8) 2.30(10) µs
^{220}Ra	(imp^b)-α_1^a-α_2-α_3	7.46(1) 19(3) ms	7.453(7) 18(2) ms
^{216}Rn	α_1-α_2^a-α_3	8.05(2) 29(4) µs	8.050(10) 45(5) µs
^{212}Po	α_1-α_2-α_3^a	8.78(2) 0.35(6) µs	8.78486(12) 0.299(2) µs
^{219}Fr	(imp^b)-α_1^a-α_2-α_3	7.32(1) 28(3) ms	7.3123(18) 20(2) ms
^{215}At	α_1-α_2^a-α_3	8.02(1) 37(3) µs	8.026(4) 100(20) µs
^{221}Ra	(imp^b)-α_1^a-α_2-α_3	6.76(1) 16(2) s	6.754(5) 28(2) s
^{217}Rn	α_1-α_2^a-α_3	7.74(1) 0.67(6) ms	7.741(2) 0.54(5) ms
^{213}Po	α_1-α_2-α_3^a	8.37(1) 3.5(3) µs	8.376(3) 3.72(2) µs

^{a}Step corresponding to the isotope that is analyzed.
^{b}Step in the correlation search that was merely used to estimate the half-life.

D. Decay chains starting from ^{220}Ra and its odd-A neighbouring isotopes ^{219}Fr, ^{221}Ra

Besides the ^{219}Ra and ^{215}Rn decays, several different α-decay chains with one or two short-lived constituents were attainable in the experimental data set. These were decay paths starting with the even-even ^{220}Ra and with its odd-A neighbouring isotopes ^{219}Fr and ^{221}Ra. Table III compares measured decay energies of main branches, in these cases corresponding to ground-to-ground state decays, and half-lives for the decay-chain members. Energies were determined on the basis of α-correlation spectra such as those depicted in Fig. 3(a) and 3(d). Half-lives were calculated with a method based on an unbinned maximum likelihood estimate in the frequentist inference, however with restricted observation times incorporated [38].

FIG. 7: Single-particle energy levels for neutrons obtained with the code HFBTHO using the Skyrme functional UNE1 without pairing. The core is ^{218}Ra and the size of the basis is 14 shells. To the left of the vertical line $\beta_3 = 0$ and to the right $\beta_2 = 0.1$. Note that the shape is the same for positive and negative values of β_3, i.e. the sign of β_3 is irrelevant.

TABLE IV: Deformation and excitation energy, ΔE, for some quasi-particle states in ^{219}Ra obtained with the code HFBTHO using the Skyrme functional UNE1. The size of the basis is 18 shells.

Shell	K^π	β_2	β_3	ΔE (MeV)
$2g_{9/2}$	$3/2^+$	0.12	-0.04	0.0
$2g_{9/2}$	$5/2^+$	0.12	-0.06	0.2
$1i_{11/2}$	$1/2^+$	0.10	0.00	0.4
$2g_{9/2}$	$1/2^+$	0.15	-0.06	1.1
$2g_{9/2}$	$7/2^+$	0.10	-0.04	1.1
$2g_{9/2}$	$9/2^+$	0.08	-0.04	1.4
$1i_{11/2}$	$11/2^+$	-0.05	0.00	1.6

Table III shows that the obtained energy values were congruent with published values. However, measured half-lives differ significantly, i.e. beyond the one-σ level, in the cases of ^{216}Rn [1], ^{219}Fr and ^{215}At [39, 40], ^{221}Ra [41] and for ^{217}Rn [42]. The clean data in this paper provide an argument for precise and accurate half-life values. These results indicate that a revision of the deviating half-lives, all obtained before the 1970s, is necessary.

VI. THEORETICAL CONSIDERATIONS

A. Deformation - ^{219}Ra

Assuming a spherical shape for ^{219}Ra with its 131 neutrons, the neutron Fermi level is the $2g_{9/2}$ shell. In a single-particle picture where the spin is given only by

the odd neutron, the ground-state spin and parity for the nucleus is expected to be $I^\pi = 9/2^+$. With a small quadrupole moment the odd neutron would occupy the orbital with a spin projection on the symmetry axis at $K = 5/2$; both for prolate and oblate shapes. In the strong coupling limit the ground state fulfils $I = K$. Since the ground state of ^{219}Ra is evaluated to have $I^\pi = 7/2^+$ [3], this state is probably neither spherical nor strongly coupled.

To date, ^{219}Ra is predicted to lie at or near the limit of where stable octupole deformation is known to exist [11]. In Ref. [44] the parameters which describe quadrupole and octupole deformations, β_2 and β_3, are calculated to be $\beta_2 = 0.090$ and $\beta_3 = -0.139$, respectively, for the ground state of ^{219}Ra.

In this work, additional calculations for the shape of ^{219}Ra were performed. The code HFBTHO v2.00d [45] was employed with three Skyrme functionals SLy4 [47], SKM* [48] and UNE1 [49]. The default pairing interactions were used for all the Skyrme functionals. Both the SLy4 and the SKM* calculations resulted in a spherical shape for the ground state of ^{219}Ra. In contrast, the UNE1 calculation showed both quadrupole and octupole deformations. A Nilsson diagram for the UNE1 calculations is shown in Fig. 7. Here calculated single-particle energies for neutrons at the Fermi level in ^{218}Ra are shown. Guided by the values given in Ref. [44], β_2 was fixed to 0.1 to the right of the vertical line in Fig. 7. The trend in the figure is that the $2g_{9/2}$ shell decreases in energy with octupole deformation whereas the $1i_{11/2}$ shell increases in energy. This result suggests that nuclei with Fermi levels at the $2g_{9/2}$ shell, which is the case for ^{219}Ra, may favor static octupole deformation. Further, this is in general agreement with the fact that octupole deformation becomes important above closed shells in heavy nuclei where shells with $\Delta l = 3$ come together. It is these shells which couple strongly through the octupole potential term as illustrated e.g. in Fig. 2 of Ref. [46].

In Table IV, calculated deformations with the HFBTHO code and the UNE1 functional are presented. The table includes all the orbitals in the $2g_{9/2}$ shell and the lowest $1i_{11/2}$ orbital at prolate and oblate shape. In agreement with Ref. [44], the obtained ground state of ^{219}Ra assumes an octupole deformation. However, the octupole deformation β_3 is smaller compared to the previous calculation.

In a previous study of this nucleus, Ref. [50] arrives at $K = 1/2$ for the odd neutron in the ^{219}Ra ground state. Here, a spin-parity of $7/2^+$ is obtained through a coupling of the odd neutron with an octupole deformed core. Thus, in order to understand the experimental states a more careful treatment of the dynamics of the angular-momentum coupling is needed.
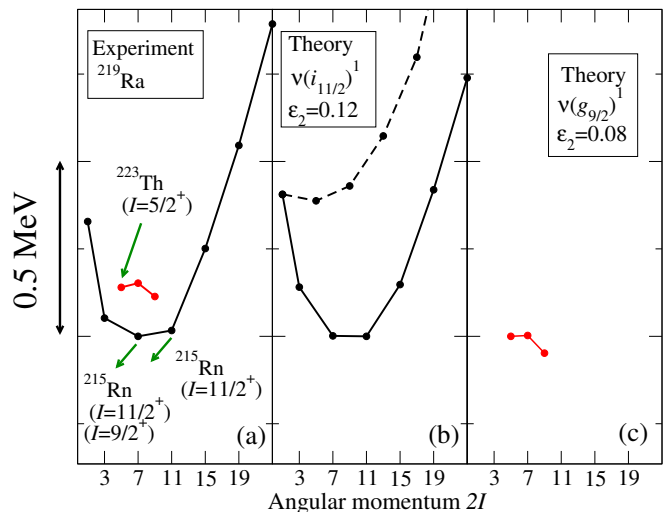

FIG. 8: Calculated and experimental low-lying states in ^{219}Ra. The experimental 328.3 keV state has undetermined angular momentum but connects to the $I = 3/2^+$ state through a quadrupole transition. In panel (a) this state is shown at $I = 1/2^+$. Arrows indicate decay by α emission.

B. Dynamics of angular-momentum coupling in ^{219}Ra

The Skyrme calculations predict the low-lying states in ^{219}Ra to be built with the odd neutron in the $g_{9/2}$ and $i_{11/2}$ shells at prolate and slightly octupole deformed shapes. At the small deformations predicted, the resulting rotational bands may be of decoupled character [51]. We employ the many-particle+rotor model of Ref. [52] to investigate the dynamics of the angular momentum coupling. As a model space we use the 14 lowest deformed valence neutron orbitals above the $N=126$ gap. This choice captures all the main Nilsson orbitals originating from the $g_{9/2}$ and $i_{11/2}$ shells. In this model space we consider five neutrons interacting with a seniority pairing force (G=0.1) [53] that can couple with a rigid deformed rotor described by moment of inertia parameters of hydrodynamical type as employed e.g. in Ref. [54]. The mean-field potential is of the modified oscillator type using the so-called standard parameters [55] and with the shape of the potential parametrized by $(\epsilon_2, \gamma, \epsilon_4)$.

With a small prolate deformation of $\epsilon_2 = 0.12$ the lowest states that have largest amplitude with the odd neutron in the $i_{11/2}$ shell are shown in Fig. 8(b). At this small deformation and with a large angular momentum for the odd neutron, the result is a decoupled band with a minimum for $I = 11/2^+$. Considering a smaller deformation of $\epsilon_2 = 0.08$ and extracting the lowest states with largest amplitude for the odd neutron in the $g_{9/2}$ orbital, one obtains the sequence of states shown in Fig. 8(c). This band starts with the odd neutron in the $g_{9/2}$ orbital with $K = 5/2$ and is drawn until the odd neutron is fully aligned at $I = 9/2^+$.

One possible interpretation of the observed states

shown in Fig. 8(a) is that the yrast isomer state at $I = 11/2^+$ is composed mainly of the odd neutron in the $K = 1/2$ orbital of the $i_{11/2}$ shell. This explains the observed α decay into mainly the spherical $i_{11/2}$ state in the daughter nucleus. The observed ground state with $I = 7/2^+$ could be a result of band mixing between the bands in panels (b) and (c). This gives a natural explanation for the observed α decay from this state into both the spherical $i_{11/2}$ state and $g_{9/2}$ states in the daughter nucleus.

The interpretation of the ground state as part of a decoupled $i_{11/2}$ band is consistent with an earlier study employing a reflection asymmetric particle-rotor model [50]. Including reflection asymmetry gives a more complete description of the spectra where the parity doublet band (not shown in Fig. 1) can also be reproduced. However, the general features of decoupling within this band appears to be independent of the octupole deformation. Calculations for the mother nucleus ^{223}Th were carried out in Ref. [50]. The $I = 5/2^+$ ground state was explained as built on a $K = 5/2$ orbital with deformations in the vicinity of $\beta_2 = 0.1$ and $\beta_3 = 0.1$. This orbital originates from the $g_{9/2}$ shell with admixtures of the $j_{15/2}$ shell due to the octupole coupling. In ^{223}Th, the resulting ground-state band follows a $\Delta I = 1$ sequence characteristic of strong coupling. A strongly coupled band is also obtained from our calculations for the $g_{9/2}$ band in ^{219}Ra if the quadrupole deformation is slightly increased. A similar origin of the $I = 5/2^+$ states in both nuclei fits well with the observed α decay between these states having a very low hindrance factor.

C. Shell model calculations of ^{215}Rn

Shell-model calculations have been performed using the code NuShellX [56] on ^{215}Rn with its four valence protons and three valence neutrons outside the doubly-magic core ^{208}Pb. Besides ^{215}Rn, other odd-mass nuclei with $A = 211-215$ have also been considered to gain confidence in the results of the conducted shell-model calculations. To access the series of nuclei located 'North-East' of ^{208}Pb in the chart of nuclides, a residual proton particle and neutron particle Kuo-Herling interaction, modified to better agree with experimental spectra, denoted "jj67pn" [57, 58] was employed. The active model space comprises the single particle proton orbitals $1h_{9/2}$, $2f_{7/2}$, $2f_{5/2}$, $3p_{3/2}$, $3p_{1/2}$, and $1i_{13/2}$, as well as neutron particles in the orbitals $1i_{11/2}$, $2g_{9/2}$, $2g_{7/2}$, $3d_{5/2}$, $3d_{3/2}$, $4s_{1/2}$, and $1j_{15/2}$.

Figure 4(b) presents the calculated levels. Similar to the level scheme deduced in the current work but in contrast to the evaluated level scheme the levels at 214 keV and 291 keV are absent in the shell-model calculations. Further, it is natural to assign the $7/2^+$ state at 333 keV to the 445 keV level in the present experimental level scheme. The first $13/2^+$ and $15/2^+$ states in the shell model calculations have been observed in a high-spin ex-

TABLE V: Comparison between revised experimental data of the present work and theoretical α-decay calculations for the ^{219}Ra→^{215}Rn decay. Only the three major α-decay branches are considered and tentative spin assignments of the initial (I_i^π) and final (I_f^π) states are given in the first two columns. The decay rates are given as: $\lambda = I_\alpha \ln(2)/t_{1/2}$ where I_α denotes the branching ratio. The branching ratios and the half-life of the $11/2^+$ state have been taken from Table II. The half-life of the combined $9/2^+$-decays was calculated to $8(3)\,\mu$s.

I_i^π	I_f^π	E_α (MeV)	λ_{exp} (s^{-1})	λ_{th} (s^{-1})
$7/2^+$	$9/2^+$	7.98	48(20)	1.4
	$11/2^+$	7.66	39(17)	0.09
$11/2^+$	$9/2^+$	–	–	0.09
	$11/2^+$	7.68	69(21)	85

periment at 570 keV and 946 keV, respectively [59]. Finally, the highest $7/2^+$ state in the calculation matches fairly well the observed 806 keV excited state in ^{215}Rn.

The shell-model predictions for single-particle partitions of the $9/2^+$ ground state (70% $\nu g_{9/2}$) as well as the $11/2^+$ (50% $\nu i_{11/2}$) and $7/2^+$ (56% $\nu g_{7/2}$) yrast states in ^{215}Rn indicate rather pure single-particle character of these states. As expected, wave-function purity further increases towards ^{208}Pb. For instance, the $9/2^+$ ground state of ^{211}Po is predicted to have 91% $\nu g_{9/2}$ character, giving rise to the known ground-state to ground-state alpha decay ^{215}Rn→^{211}Po.

D. α-decay calculations of ^{219}Ra

Calculations of α-decay rates for ^{219}Ra have been conducted in accordance with the method described in Ref. [60]. The method assumes spherical shapes for both the mother and the daughter nuclei. The Skyrme functional SLy4 is used together with the mixed pairing. States in even-Z odd-N nuclei connected by α decays are described as single quasi-neutron excitations of an even-even Hartree-Fock-Bogoliubov vacuum. The Coulomb penetrability is evaluated using the experimental E_α values. As a consistency test, the method has been used to calculate the half-life of the ^{215}Rn ground state which α decays unhindered to the ground state of ^{211}Po. Both these states are known to be spherical and have $I^\pi = 9/2^+$. The calculations yield a half-life of 3.8 μs, which fits well with the experimental value of 2.3(10) μs.

Table V presents α-decay rates for both the ground state and the isomeric state in ^{219}Ra entering the two states $9/2^+$ and $11/2^+$ in ^{215}Rn. For the ground and isomeric state, in order to fit with the experimental values of the spin and parity, the quasi-neutron was put into the $2g_{7/2}$ and $1i_{11/2}$ shells, respectively, despite the $2g_{7/2}$ shell being high above the Fermi level, i.e. it is not realistic that the odd neutron is placed there. However, it

is the only nearby spherical shell with the ground state spin-parity: $7/2^+$. As can be seen in the table, the calculated rates differ by more than two orders of magnitude from the experimental values for the $7/2^+$ ground-state decay channels. This disagreement is yet another indication that the ground state of ^{219}Ra has a more complicated non-spherical structure. Further, if the $11/2^+$-state in ^{219}Ra is approximated as spherical it α-decays unhindered to the $11/2^+$-state in ^{215}Rn with a decay rate that is only slightly larger than the experimental value. Hence, the α-decay calculations support the idea of a weakly-deformed isomeric state built on the $1i_{11/2}$ shell in ^{219}Ra.

Finally, we suggest that the two observed branches namely the $7/2^+ \rightarrow 9/2^+$ and $7/2^+ \rightarrow 11/2^+$ decays can be explained as a result of configuration mixing in the mother nucleus as discussed in Sec. VI B.

VII.   CONCLUDING REMARKS

The ^{219}Ra$\rightarrow^{215}$Rn decay has been closely studied by means of α-γ spectroscopy. As a main result, an α-decay branch from the excited state at 17 keV in ^{219}Ra is proposed to resolve a discrepancy between the evaluated level scheme and the experiment. This 17-keV state in ^{219}Ra was unknown in previous decay spectroscopy experiments. Our results are consistent with Geant4 simulations, and further support the debated ground-state spin of ^{219}Ra, its first excited state, as well as the low-lying levels in ^{215}Rn. Contemporary theoretical calculations on deformation, rotational states and the α decay justify the nuclear structure interpretation. Despite the large data set used in the current study, the α-γ coincidence yield for the ^{219}Ra$\rightarrow^{215}$Rn decay is limited. To gain more confidence in the nuclear structure interpretation further similar experimental studies are encouraged.

The deployment of the pile-up pulse analysis routine and the correlation analysis in this work enable the study of short-lived α-decaying nuclei in experiments with reactions similar to ^{48}Ca + ^{243}Am. Beyond the ^{219}Ra$\rightarrow^{215}$Rn decay, further decay chains were studied. The results show that the measured half-lives differed significantly in the cases of the ^{216,217}Rn, ^{219}Fr, ^{215}At and ^{221}Ra α decays and a revision of the evaluated half-lives – from measurements made before 1970 – is suggested.

[1] K. Valli, E. K. Hyde and J. Borggreen, Phys. Rev. C **1**, 2115 (1970).
[2] R. L. Hahn, M. F. Roche, and K. S. Toth, Phys. Rev. **182**, 4 (1969).
[3] Evaluated Nuclear Structure Data File (ENSDF), http://www.nndc.bnl.gov/ensdf/ (2018).
[4] E. Browne, Nucl. Data Sheets **93**, 802 (2001).
[5] S. K. Basu, G. Mukherjee, B. Singh, Srijit Bhattacharya, A. De, D. Mondal, Nucl. Data Sheets **114**, 2023 (2013).
[6] A. M. Y. El-Lawindy et al., J. Phys. G: Nucl. Phys. **13**, 93 (1987).
[7] R. K. Sheline, C. F. Liang, P. Paris, A. Gizon, and V. Barci, Phys. Rev. C **49**, 725 (1994).
[8] E. D. Hackett, J. A. Kuehner, J. C. Waddington, and G. D. Jones. Phys. Rev. C **40**, 1234 (1989).
[9] P. D. Cottle et al., Phys. Rev. C **36**, 2286 (1987).
[10] M. Wieland et al., Phys. Rev. C **45**, 1035 (1992).
[11] P. A. Butler and W. Nazarewicz, Rev. Mod. Phys. **68**, 349 (1996).
[12] L. A. Riley et al., Phys. Rev. C **62**, 021301(R) (2000).
[13] C. F. Liang et al., Z. Phys. A **341**, 401 (1992).
[14] Phil Walker and George Dracoulis, Nature **399**, 35 (1999).
[15] Ulrika Forsberg, PhD thesis, Lund University, ISBN 978-91-7623-813-4 (pdf).
[16] D. Rudolph et al., Phys. Rev. Lett. **111**, 112502 (2013).
[17] U. Forsberg et al., Nucl. Phys. **A 953**, 117 (2016).
[18] S. Agostinelli et al., Nucl. Instrum. Meth. **A 506**, 250 (2003).
[19] J. M. Gates et al., Phys. Rev. C **83**, 054618 (2011).
[20] M. Schädel et al., Eur. Phys. J. D, **45**, 67 (2007).
[21] A. Semchenkov et al., Nucl. Instrum. Meth. **B 266**, 4153 (2008).
[22] L.-L. Andersson et al., Nucl. Instrum. Meth. **A 622**, 164 (2010).
[23] J. Khuyagbaatar et al., Phys. Rev. Lett. **115**, 242502 (2015).
[24] J. Hoffmann et al., GSI Scientific Report 2011, GSI Report 2012-1 (2012).
[25] S. N. Liddick et al., Phys. Rev. Lett. **97**, 082501 (2006).
[26] T. H. Huang et al., Phys. Rev. C **96**, 014324 (2017).
[27] M. D. Sun et al., Phys. Lett. **B 771**, 303 (2017).
[28] A. Georgiev and W. Gast, IEEE Transactions on Nuclear Science **40**, 4 (1993).
[29] V. T. Jordanov, G. F. Knoll, A. C. Huber, and J. A. Pantazis, Nucl. Instrum. Meth. **A 353**, 261 (1994).
[30] R. Grzywacz, Nucl. Instrum. Meth. **B 204**, 649 (2003).
[31] Martin Lauer, PhD Thesis, University of Heidelberg, CERN-THESIS-2004-047.
[32] Victor Ionut Stoica, PhD Thesis, University of Groningen, UMCG Research Database (2012).
[33] Anton Roth, Master Thesis http://lup.lub.lu.

se/student-papers/record/8882017, Lund University (2016).

[34] T. Kibédi, T. W. Burrows, M. B. Trzhaskovskaya, P. M. Davidson, and C. W. Nestor Jr, Nucl. Instrum. Meth. **A 589**, 202 (2008).

[35] L.G. Sarmiento, L.-L. Andersson, and D. Rudolph, Nucl. Instrum. Meth. **A 667**, 26 (2012).

[36] D. Rudolph *et al.*, Acta Phys. Pol. **B 45**, 263 (2014).

[37] U. Forsberg *et al.*, Acta Phys. Pol. **B 43**, 305 (2012).

[38] X. C. Chen, Q. Zeng, Yu. A. Litvinov, X. L. Tu, P. M. Walker, M. Wang, Q. Wang, K. Yue, and Y. H. Zhang, Phys. Rev. C **96**, 034302 (2017).

[39] G. Bastin and C F. Leang and R. J. Walen, J. Phys.(Paris) Suppl.No.1, Colloq.C1-181 (1968).

[40] G. Graeffe and P. Kauranen, J. Inorg. Nucl. Chem. **28**, 933 (1966).

[41] P. A. Tove, Arkiv Fysik, **13** (1958).

[42] C. P. Ruiz, Technical Report, Lawrence Radiation Laboratory, Berkeley, UCRL-9511 (1961).

[43] C. Qi, F. R. Xu, R. J. Liotta, R. Wyss, M. Y. Zhang, C. Asawatangtrakuldee, and D. Hu, Phys. Rev. C **80**, 044326 (2009).

[44] P. Möller, A. J. Sierk, T. Ichikawa, and H. Sagawa, arXiv:1508.06294v1 [nucl-th], (2015).

[45] M. V. Stoitsov, N. Schunck, M. Kortelainen, N. Michel, H. Nam, E. Olsen, and S. Wild, Comp. Phys. Commun. **184**, 1592 (2013).

[46] W. Nazarewicz, P. Olanders, I. Ragnarsson, J. Dudek, G. A. Leander, P. Mö ller, and E. Ruchowska.

[47] E. Chabanat, P. Bonche, P. Haensel, J. Meyer, and R. Schaeffer, Nucl. Phys. **A 627**, 710 (1997).

[48] J. Bartel, P. Quentin, M. Brack, C. Guet, and H.-B. Håkansson, Nucl. Phys. **A 386**, 79 (1982).

[49] M. Kortelainen, J. McDonnel, W. Nazarewicz, P.-G. Reinhard, J. Sarich, N. Schunck, M. V. Stoitsov, and S. M. Wild, Phys. Rev. C **85**, 024304 (2012).

[50] G. A. Leander and Y. S. Chen, Phys. Rev. C **37**, 2744 (1988).

[51] F. S. Stephens, Rev. Mod. Phys. **47**, 43 (1975).

[52] B. G. Carlsson and I. Ragnarsson, Phys. Rev. C **74**, 044310 (2006).

[53] S.-G. Nilsson and I. Ragnarsson, *Shapes and Shells in Nuclear Structure*, Cambridge University Press 1995.

[54] S. E. Larsson, G.A. Leander, I. Ragnarsson, Nucl. Phys. **A 307**, 189 (1978).

[55] T. Bengtsson and I. Ragnarsson, Nucl. Phys. **A 436**, 14 (1985).

[56] B. A. Brown and W. D. Rea, Nucl. Data Sheets **120**, 115 (2014).

[57] J. B. McGrory and T. T. S. Kuo, Nucl. Phys. **A 247**, 283 (1975).

[58] E. K. Warburton and B. A. Brown, Phys. Rev. C **43**, 602 (1991).

[59] M. E. Debray *et al.*, Phys. Rev. C **86**, 014326 (2012).

[60] D. E. Ward, B. G. Carlsson, and S. Åberg, Phys. Rev. C **92**, 014314 (2015).

Nucl. Phys. **A 429**, 269 (1984).